Geophys. J. Int. (1998) **134**, 596–612

Radiative transfer and diffusion of waves in a layered medium: new insight into coda Q

Ludovic Margerin,[1] Michel Campillo[1,2] and Bart van Tiggelen[3]

[1] *Laboratoire de Géophysique Interne et Tectonophysique, Observatoire de Grenoble, Université Joseph Fourier,* BP 53, 38041 *Grenoble Cedex 9, France. E-mail: lmarger@lgit.obs.ujf-grenoble.fr*

[2] *Institut Universitaire de France, France*

[3] *Laboratoire de Physique et Modélisation des Systèmes Condensés, Maison des Magistères Jean Perrin* CNRS BP 66, 38042 *Grenoble Cedex, France*

Accepted 1998 March 16. Received 1998 January 26; in original form 1997 July 17

SUMMARY

This paper is devoted to the study of the seismic coda in inhomogeneous media exhibiting a discontinuity of physical properties at a given depth. We focus on the problem of a layer overlying a half-space and analyse the precise effect of a contrast of wave velocities and/or scattering strengths between them. In order to model *S*-coda-wave envelopes, we solve the Radiative Transfer Equation by the Monte Carlo method, thereby neglecting the polarization (i.e. the acoustic approximation). We pay special attention to the transition towards the diffusion regime. Under the assumption of an almost isotropic intensity field, a Diffusion Equation can be derived from the Radiative Transfer Equation and we accurately determine the boundary conditions associated with our models. Analytical solutions of the Diffusion Equation have been obtained and systematically compared to the numerical solutions of the Radiative Transfer Equation. We identify the domain of validity of the diffusion approximation which provides a simple analytical form for the decay in the late coda.

We apply our theoretical investigations to the continental lithosphere. If the scattering strengths of the mantle and the crust are assumed to be of the same order, a velocity contrast at the Moho will—according to our theory—amplify the coda signal, since part of the energy is trapped in the crust. An amplification factor is defined and given explicitly as a function of the reflection coefficients and the velocity contrast at the Moho. The shape of the long time decay is of the algebraic form $t^{(-3/2)}$, like that of a uniform half-space.

On the other hand, if the scattering strength of the mantle is small with respect to that of the crust, the decay in the diffusive regime is predicted to be of the form $t^{-1}\exp(-2\pi ft/Q_c^*)$, where Q_c^* is a function of the reflection coefficients at the Moho, the mean free path of waves in the crust, and frequency f. The coefficient Q_c^* quantifies the rate at which the partially trapped energy leaks from the crust into the mantle. This formula has the same form as that proposed by Aki & Chouet (1975) to fit coda observations, which has since been widely used to deduce the Q_c parameter. With realistic model parameters, we find that Q_c^* roughly equals the parameter Q_c deduced from observations. This shows that the effect of partial trapping of energy in the crust may be significant. Consequently, seismic albedos of the crust may have been underestimated in previous studies. In our theory, the energy decay of seismic coda waves is determined by the layered structure of the Earth, that is a highly heterogeneous crust overlying a rather homogeneous mantle. Such structure is confirmed by geological and geochemical studies.

Key words: layered media, Q, scattering, seismic coda.

INTRODUCTION

Observations show that the waves forming the tails of seismograms follow complicated paths in the Earth's lithosphere. Aki & Chouet (1975) demonstrated that the time decay of these so-called coda waves is a characteristic of the underlying medium, independent of the source or the site conditions at the station. By interpreting these arrivals as scattered waves

on randomly distributed heterogeneities in the lithosphere and using two different approximations (single scattering and diffusion), they proposed an expression for the coda decay in terms of the attenuating properties of the Earth's lithosphere.

The existence of a coda has been recognized on different time- and length scales in various areas of physics where multiple scattering occurs. Although the typical wavelengths for optics, acoustics and seismology are microns, centimetres and hundreds of metres respectively, a similar theoretical framework can be used for all these fields. Coda is widely accepted as the result of multiple scattering in a disordered medium, especially in optics. More than forty years ago, Chandrasekhar (1950) developed the phenomenological theory of radiative transfer (Radiative Transfer), solving the problem of energy propagation in a random medium, using the basic assumption that the phase of scattered waves is randomized by the many scattering events so that no interference occurs. Since then, several authors have successfully established the link between the wave and Radiative Transfer equations (Burridge & Papanicolaou 1975; Turner & Weaver 1994; Ryzhik Papanicolaou & Keller 1996).

When $ka \ll 1$ (where k is the wavenumber and a is a typical correlation length of the fluctuations), perturbation theory provides an expansion of the Green function G of the inhomogeneous medium. Averaging G and GG^* over all realizations of the random medium, the Dyson equation governing the mean field and the Bethe–Salpeter equation governing its covariance can be obtained (Frisch 1968). The latter is basically equivalent to a radiative transfer equation once the so-called 'ladder approximation' (Rytov, Kravtsov & Tatarskii 1989, Sheng 1995) is adopted. The theory turns out to be applicable for a wide range of parameters, only excluding the regime of localization (Ryzhik *et al.* 1996).

Several solutions of the Radiative Transfer Equation pertaining to seismic waves have been published and their relevance to seismology has been realized (Abubakirov & Gusev 1990; Hoshiba 1991; Zeng, Su & Aki 1991; Sato 1995). They have been used in attempts to estimate the seismic albedo and the scattering mean free path from seismic data. So far, in the interpretation of the data, the underlying assumption has been that the Earth can be considered as an infinite medium with homogeneous wave velocities and statistical properties. However, several authors have suggested that the scattering and absorption properties of the Earth may vary with depth (Rautian & Khalthurin 1978; Abubakirov & Gusev 1990; Hoshiba 1994; Gusev 1995).

In this paper, we would like to get some insight into the time decay of coda waves in continental domains for local as well as regional earthquakes. To this end, we solve the acoustic Radiative Transfer Equation by the Monte-Carlo method, taking into account two major boundary conditions: the surface of the Earth which perfectly reflects energy and an angle-dependent reflection coefficient at the Moho interface due to the difference of wave velocities in the crust and the mantle. No P–S or S–P mode conversions have been taken into account in our scalar analysis. In addition, we assume that earthquakes occur just below the surface, which is in agreement with the observed shallow seismogenic zone in continental areas. Another question we want to address is the convergence of the multiple scattering towards the diffusion limit. We systematically compare our numerical solutions to analytical solutions of the diffusion equation. This enables us to define the domain of validity of the diffusion approximation (Diffusion Approximation). It is important to note that inside the Earth the causes for multiple scattering are numerous: random velocity fluctuations, cracks and cavities. Each scattering process has its own mean free path. Quite conveniently the Diffusion Equation characterizes the entire scattering process with only two parameters, the diffusion constant D of the waves and the transport mean free path ℓ^* (related by $D = v\ell^*/3$, where v is the shear-wave speed), and we do not need to know the microscopic details of the Earth structure.

RADIATIVE TRANSFER IN A LAYERED MEDIUM

In this section we present the geometries and physical properties of our different models, and explain our numerical scheme to solve the Radiative Transfer Equation.

Description of the models

To a first-order approximation, the continental lithosphere can be regarded as a horizontally stratified medium with depth-dependent properties. A well-known feature of continental areas is the Moho, which separates the low-velocity crust from the high-velocity mantle. To understand how a plane structure affects the decay of coda signals, we apply the Radiative Transfer theory to a simplified layered medium. In such a medium physical properties can be different in the upper and lower parts of the medium, as explained below.

Let us recall the parameters relevant to the description of multiple scattering. The acoustic Radiative Transfer Equation for a statistically isotropic medium without absorption is

$$\frac{1}{v}\frac{\partial I(\boldsymbol{x}, \boldsymbol{\Omega}, t)}{\partial t} + \boldsymbol{\Omega}\cdot\nabla_x I(\boldsymbol{x}, \boldsymbol{\Omega}, t) = -\frac{I(\boldsymbol{x}, \boldsymbol{\Omega}, t)}{l} + \frac{1}{4\pi l}\int_{4\pi} d\Omega\, p(\boldsymbol{\Omega}, \boldsymbol{\Omega}') I(\boldsymbol{x}, \boldsymbol{\Omega}', t) + e(\boldsymbol{x}, \boldsymbol{\Omega}, t) \tag{1}$$

(e.g. Chandrasekhar 1950).

We use the following notation.

I is the specific intensity, which is the amount of energy flowing across a surface in a specified direction per unit time, per unit solid angle and per unit surface. It is a function of:

$\boldsymbol{x}$, the position in some reference frame;

$\boldsymbol{\Omega}$, a unit vector in the direction of propagation;

t, the time of observation.

∇_x denotes derivatives are performed on the position variable $\boldsymbol{x}$.

$\int_{4\pi} d\Omega$ denotes integration over all directions of space.

$p(\boldsymbol{\Omega}, \boldsymbol{\Omega}')$ is the phase function which describes the angular dependence of the scattering process.

e is the source term,

v is the S-wave velocity,

l is the scattering mean free path.

All are functions of depth as explained below. It is customary to define the mean free time $\tau = l/v$ denoting the average time between two scattering events. In seismology, the observable quantity is the local, time-dependent energy density at the

surface of the Earth:

$$\rho(x, t)=\frac{1}{v}\int_{4\pi} I(x, \Omega, t)d\Omega. \quad (2)$$

The left-hand side of eq. (1) is the intensity variation of a beam of energy during propagation along Ω. The first term on the right-hand side is the loss of the incident beam in all directions due to scattering. The second term represents the reinforcement of the incident beam due to the scattered energy from direction Ω' to direction Ω. The last term denotes sources of intensity. This equation expresses the local conservation of energy. In infinite uniform media the dimensionless parameters which control the physics of the problem are r/l and t/τ, where r is the distance between the point source and the detector.

Let us focus on the problem of a layer over a half-space and discuss the physical implications. In the following, the subscripts 1 and 2 refer to the top layer and the underlying half-space respectively. The upper layer is bounded from above by a free surface that perfectly reflects energy. We suppose that the earthquake occurs at shallow depths and that the detectors are located just below the free surface. We distinguish four types of models, which differ in their relative values of the velocities v_1 and v_2 and the mean free path l_1 and l_2; H is the thickness of the layer (see Fig. 1 and Table 1). We distinguish two cases.

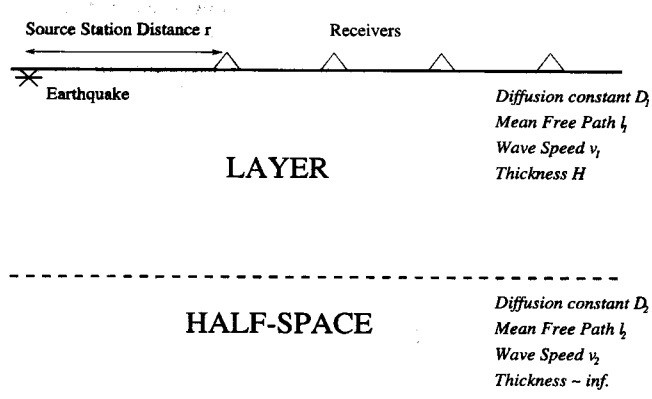

Figure 1. Geometry and physical parameters of the models. The earthquakes and receivers are assumed to be located just below the free surface. Numerical values of the physical constants can be found in Table 1.

(1) Media where scattering occurs in the whole space (models 1 and 2).

(2) Media where scattering is confined to the subsurface layer of thickness H (models 3 and 4). This corresponds to the limiting case $l_2\to\infty$. An infinite value of the mean free path physically means that no scattering occurs and that waves propagate along straight lines.

Subsequently, we distinguish media with and without a wave-velocity discontinuity at depth H. Together this leads to four different categories, as summarized in Table 1. The numbers in Table 1 will be explained later. Note that model 1 corresponds to the classical uniform half-space used by Hoshiba (1993) for data interpretation and will be considered by us as a reference model. Below, we discuss major differences with the three other cases.

(1) Due to the addition of a sharp velocity contrast between the top layer and the half-space, reflection and transmission of waves at the base of the layer must be taken into account. Hence, part of the emitted energy will be guided in the upper layer and another part will leak into the half-space.

(2) For models 3 and 4 the thickness H is the crucial length scale.

In addition to the space and time variables, the solutions of the Radiative Transfer Equation depend on the following ratios:

$\frac{l_1}{l_2}, \frac{v_1}{v_2}$ for model 2;

$\frac{H}{l_1}, \frac{v_1}{v_2}$ for models 3 and 4.

The many degrees of freedom make our model—though largely simplified—rather complex. In the next section, we discuss how the boundary conditions at the top and bottom of the layer are taken into account.

Solution of the Radiative Transfer Equation by Monte Carlo simulations

The basic procedure we use has been described in great detail by Hoshiba (1991, 1995), so we will only summarize the method and mention some important modifications we have added to deal with the interfaces. The Monte Carlo scheme is a

Table 1. Classification and physical properties of the models.

	Model 1	Model 2	Model 3	Model 4
velocity contrast	no	yes	no	yes
$\frac{v_1}{v_2}$	$\frac{3.5}{3.5}=1$	$\frac{3.5}{4.7}=0.74$	$\frac{3.5}{3.5}=1$	$\frac{3.5}{4.7}=0.74$
mean free path contrast	no	no	yes	yes
$\frac{l1}{l2}$	$\frac{10}{10}, \frac{30}{30}=1$	$\frac{10}{10}, \frac{30}{30}=1$	$\frac{10}{\infty}, \frac{30}{\infty}=0$	$\frac{10}{\infty}, \frac{30}{\infty}=0$
	$\frac{70}{70}, \frac{150}{150}=1$	$\frac{70}{70}, \frac{150}{150}=1$	$\frac{70}{\infty}, \frac{150}{\infty}=0$	$\frac{70}{\infty}, \frac{150}{\infty}=0$
relative layer thickness H/l_1				
$H=40$ km	∞	0.27, 0.57 1.33, 4.	id.	id.
$H=30$ km	∞	0.2, 0.43 1., 3.	id.	id.

discretized version of the Radiative Transfer process (see Lux & Koblinger 1991) and requires three main steps.

(1) Construction of the ith random walk of a so-called acoustic 'energy particle' in a medium with a specified geometry, where $i=1, \ldots, N$; N is the total number of random walks we wish to simulate. The particle starts at a point source and changes its direction of propagation each time it encounters either an interface or a scatterer.

(2) Definition of a lapse time window of observation such that the time origin is the energy emission in the medium and the end time is at 420 s, which is enough to study the coda of regional earthquakes. This window is divided into intervals $]n\Delta t, (n+1)\Delta t[$, where $\Delta t = 1/30$ s is a constant time increment small with respect to the mean free times, and $n=0, \ldots, 12\,600$. $\rho_i(O, n)$ denotes the time-discretized version of the energy density at a subsurface receiver located at point O. For the mth scattering event, we calculate all energy contributions $E_i^m(pp)$ of the current particle and their associated traveltimes $t_i^m(pp)$ from source to detector. pp denotes all paths from the last scatterer to the detector, including multiple reflections on the interfaces, but excluding other scattering events, and such that $t_m^i(pp) < 420$ s. These contributions are stored in $\rho_i(O, n_i^m(pp))$, where $t_i^m(pp) \in]n_i^m(pp)\Delta t, (n_i^m(pp)+1)\Delta t[$. When the traveltime of the particle exceeds the length of the observation window, the random walk is stopped and a new particle is launched at the source.

(3) Repetition of the process in order to explore all realizations of the random variables. Finally, all random walk results are averaged to obtain the energy density:

$$\rho(O, n) = \frac{1}{N} \sum_i \rho_i(O, n). \tag{3}$$

We now explain how we have taken into account interfaces during the random walk. Consider a layer (medium 1) overlying a half-space (medium 2) as shown in Fig. 1. They may have different scattering mean free paths, densities and wave speeds. In our analysis, mode conversions are neglected and shear waves are treated as acoustic waves. v_j, d_j, l_j are respectively the shear-wave velocity, density and mean free path of layer j. When a wave is incident in medium 1 on the velocity discontinuity with medium 2, it may be either reflected or refracted from the boundary, according to Snell's law. Let us call θ_1, θ_1', θ_2 the angles of incidence, reflection and refraction respectively. For $v_1 < v_2$, a critical angle $\theta_c = \arcsin(v_1/v_2)$ exists that requires special care.

Below the critical angle ($\theta_1 < \theta_c$) we have

$$\cos\theta_2 = \sqrt{1 - \left(\frac{v_1}{v_2}\right)^2 \sin^2\theta_1} \quad \text{and} \quad \theta_1 = \theta_1'. \tag{4}$$

Introducing $\zeta = d_2 v_2 \cos\theta_2 / d_1 v_1 \cos\theta_1$, we define

$$R_{12} = \left(\frac{1-\zeta}{1+\zeta}\right)^2 \tag{5}$$

and

$$1 - R_{12} = T_{12} = \frac{4\zeta}{(1+\zeta)^2}, \tag{6}$$

where one recognizes R_{12} as the energy reflection coefficient and T_{12} as the energy transmission coefficient for an acoustic plane wave incident in medium 1 on the boundary between media 1 and 2. Accordingly, when a particle in medium 1 encounters the boundary between media 1 and 2, it remains in medium 1 with a probability R_{12} and continues its walk in medium 2 with a probability T_{12}. The new direction of propagation of the particle is determined by eq. (4).

In the case where $\theta_1 > \theta_c$, one has $R_{12}=1$, $T_{12}=0$ and the particle will stay in medium 1. Note that contributions from evanescent waves are neglected in the present analysis. The phase change of the reflected wave at the interface is unimportant because, as stated earlier in the Introduction, the intensity is defined as $\langle GG^* \rangle$, the average of the product of two conjugates values. When the particle reaches the free surface it is always reflected with probability 1.

To determine the free path length FPL of a particle between two consecutive scattering events in the layered medium, we proceed as follows. Let us define $SP_{i_1}^m, SP_{i_2}^m, \ldots, SP_{i_k}^m, \ldots$, the lengths of straight paths (that is with a constant direction of propagation) of the particle i in the layered medium between the mth and $(m+1)$th scatterings (see Fig. 2). If the particle encounters a velocity discontinuity, its direction of propagation changes according to the reflection/refraction laws defined above. If not, the direction of propagation of the particle is kept constant. We select a uniformly distributed random number $\epsilon \in]0, 1[$ and determine the integer q such that

$$\sum_{k=1}^{k=q} \frac{SP_{i_k}^m}{l_{i_k}^m} = -\ln\epsilon, \tag{7}$$

where $l_{i_k}^m$ is the value of the mean free path on the kth straight path. The free path length between two consecutive scattering events is therefore

$$FPL = \sum_{k=1}^{k=q} SP_{i_k}^m, \tag{8}$$

and the corresponding traveltime T is easily calculated as

$$T = \sum_{k=1}^{k=q} \frac{SP_{i_k}^m}{v_{i_k}^m}, \tag{9}$$

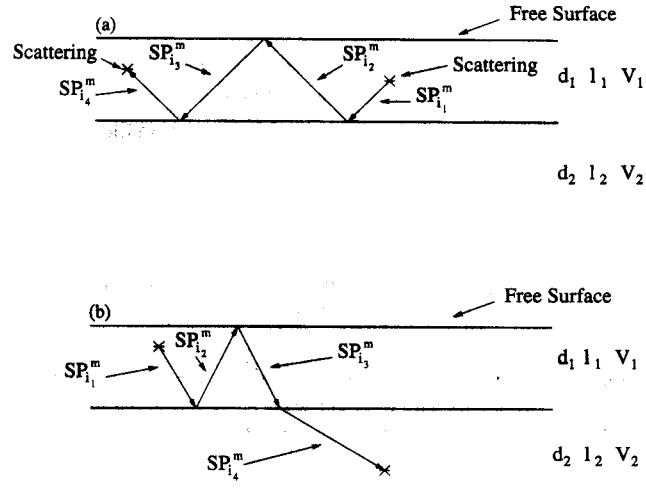

Figure 2. Determination of the free path between two successive scattering events in the layered medium. The direction of propagation of the particle changes according to Snell's law when it encounters a boundary, and is kept constant otherwise. (a) The particle remains in the layer; (b) it is transmitted in the lower half-space.

where v_k^m is the value of the S-wave speed on the kth straight path. Fig. 2(a) illustrates the case where the particle remains trapped in the layer; Fig. 2(b) illustrates the case where the particle is reflected several times from the boundaries of the layer before it is finally transmitted into the half-space. In each case $q=4$. Note that the value $m=0$ corresponds to the emission at the source and is treated in exactly the same way, because an isotropic radiation is assumed. When the mean free path in the half-space is very large, that is $l_2 \to \infty$, the particle transmitted in the lower medium will travel downwards and cannot be backscattered. Its random walk is therefore stopped and a new particle is launched at the source.

The next modification concerns the energetic contents of a particle after scattering. In principle, we have to account for all possible paths from the scatterer to the detector. However, let us begin with the simplest path. We consider a beam of energy emitted in a solid angle $(\theta_2, \theta_2+d\theta_2; \phi_2, \phi_2+d\phi_2)$ from a scatterer S located in the half-space, where θ and ϕ are the angular spherical coordinates (see Fig. 3). Once the beam has crossed the interface separating the layer and the half-space its direction of propagation has changed to $(\theta_1, \theta_1+d\theta_1; \phi_1, \phi_1+d\phi_1)$ because of the refraction and it directly reaches a point-like detector O in the layer. If we call dS_2 and dS_1 the cross-sections of the beam at I (the intersection point at the base of the layer) and O respectively, the ratio dS_1/dS_2 is different from that for the uniform case because the geometrical spreading of the beam is modified by the refraction. This is the fundamental modification compared to a model with uniform velocity. The energy density contribution of the particle is calculated in the following way.

The probability of scattering in the solid angle $(d\theta_2, d\phi_2)$ is $p(\cos\chi)(dS_2)/(4\pi SI^2)$, where χ is the cosine of the scattering angle and p is the phase function.

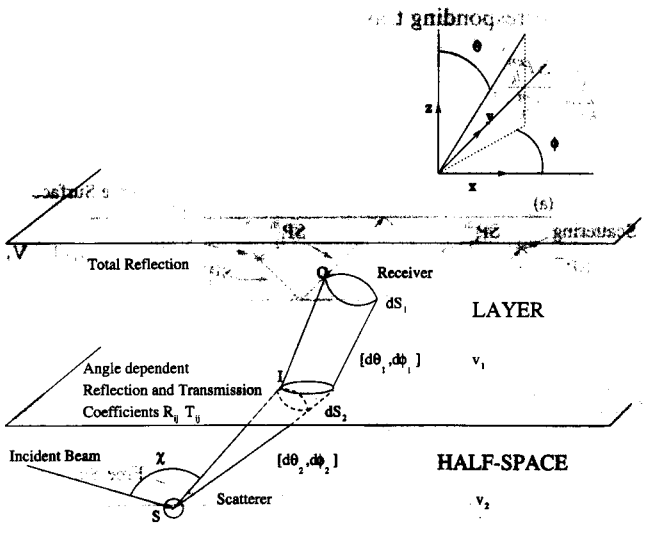

Figure 3. Transmission of a scattered energy beam at an interface separating two media with different wave speeds. S is the location of the scattering event. I is a point on the intersection surface between scattered beam and interface. O is the location of the detector. χ denotes the angle between the incident and scattered directions. The beam is composed of scattered energy in the solid angle $(d\theta_2, d\phi_2)$ measured from the point S, where θ and ϕ represent angular spherical coordinates. At point I, the cross-section of the beam is dS_2. Once the beam crosses the interface, the new solid angle is $(d\theta_1, d\phi_1)$. At point O, the cross-section of the beam is dS_1.

The probability of transmission is $T_{21}(\theta_2)$, where T_{21} is the transmission coefficient for a plane wave incident from medium 2 on the boundary between media 1 and 2.

The probability that no other scattering event occurs on the path from S to O is $\exp[-(SI/l_2)-(IO/l_1)]$.

We impose the following angular relations:

$$d\phi_1 = d\phi_2 \quad \text{and} \quad \frac{\cos\theta_1 d\theta_1}{v_1} = \frac{\cos\theta_2 d\theta_2}{v_2}. \tag{10}$$

Geometrical considerations show that

$$dS_2 = SI^2 \sin\theta_2 d\theta_2 d\phi_2, \tag{11}$$

$$dS_1 = (SI\sin\theta_2 + IO\sin\theta_1)\left(IOd\theta_1 + SId\theta_2 \frac{\cos\theta_1}{\cos\theta_2}\right). \tag{12}$$

The volume swept by the energy beam during the time interval dt is $dS_1 v_1 dt$.

Finally, we obtain the energy contents of the direct beam:

$$E_0 = \frac{p(\cos\chi)T_{21}(\theta_2)\exp\left(-\dfrac{SI}{l_2}-\dfrac{IO}{l_1}\right)}{v_1 dt\left(SI\dfrac{\cos\theta_1}{\cos\theta_2}+IO\dfrac{v_1\cos\theta_2}{v_2\cos\theta_1}\right)\left(SI+IO\dfrac{v_1}{v_2}\right)4\pi}. \tag{13}$$

Other paths from the scatterer to the receiver are possible. They involve multiple reflections between the top and bottom of the layer, excluding other scattering events. Accounting carefully for the reflection and transmission coefficients, a straightforward modification of the formula (13) enables us to calculate the energy contributions of all these paths. A similar Monte Carlo scheme has been developed by Hoshiba (1997) to study the effect of the focal depth in depth-dependent velocity structures. We checked the validity of our code by comparing our results with published solutions for simple configurations. The agreement with the results presented by Hoshiba (1995, 1997) is perfect.

DIFFUSION APPROXIMATION

Derivation of the Diffusion Equation

Multiple scattering processes will tend to uniformize the angular dependence of the intensity because each scattering event distributes energy in all directions of space. Hence, after a sufficiently large number of scattering events, the intensity will only slightly differ from isotropy. In the theory of Radiative Transfer it is customary to introduce the current vector $\boldsymbol{J}(\boldsymbol{x}, t) = \int_{4\pi} I(\boldsymbol{x}, t)\boldsymbol{\Omega} d\Omega$ so that $\boldsymbol{J}(\boldsymbol{x}, t)\cdot\boldsymbol{n}dS$ gives the rate of flow of energy across the surface dS with normal $\boldsymbol{n}$. At each point $\boldsymbol{x}$, the current vector gives the direction of maximum energy flow. The physical idea of the Diffusion Approximation is to write the intensity as a sum of two terms: first its angularly averaged value, and second a term which takes into account the slight deviation from isotropy expressed by the current vector. Mathematically, this implies that at each point the intensity is only a function of the cosine of the angle $(\boldsymbol{J}, \boldsymbol{\Omega})$. In term of $\boldsymbol{J}$ and ρ the intensity is

$$I(\boldsymbol{x}, \boldsymbol{\Omega}, t) = \frac{\rho v}{4\pi}(\boldsymbol{x}, t) + \frac{3}{4\pi}\boldsymbol{J}(\boldsymbol{x}, t)\cdot\boldsymbol{\Omega} + \ldots \tag{14}$$

(e.g. Kourganoff 1967). One recognizes here the first two terms of an expansion of the intensity in a Legendre series. The Diffusion Approximation ignores terms of higher order. We

shall now derive two equations by integrating the Radiative Transfer Equation over all solid angles. We first apply the following operator: $\int_{4\pi}(.)d\Omega$ and we also assume that the source is isotropic and point-like (which will be the case in all our simulations). We obtain the following expression, sometimes called the 'continuity equation' owing to its similarity with the continuity equation of fluid mechanics:

$$\frac{\partial \rho(x, t)}{\partial t} + \nabla \cdot J(x, t) = \delta(x - x_0)\delta(t). \tag{15}$$

An exact consequence of eq. (15) is that the variation in the amount of energy in a volume V is due to the flow across its boundaries plus the local production. Next we apply the vectorial operator $\int_{4\pi}(.)\Omega d\Omega$ to the Radiative Transfer Equation and make use of eq. (14) to evaluate the second term on the left-hand side:

$$\frac{v}{3}\nabla\rho(x, t) + \frac{1}{v}\frac{\partial J(x, t)}{\partial t} = -\frac{J(x, t)}{l}(1 - \langle\cos\theta\rangle), \tag{16}$$

where brackets denote averaging over all solid angles,

$$\langle\cos\theta\rangle = \frac{1}{4\pi}\int_{4\pi} p(\cos\theta)\cos\theta\, d\Omega, \tag{17}$$

and p is the phase function that describes the angular dependence in single scattering. By neglecting the derivative of the current vector with respect to time, we obtain the so-called Fick's law:

$$J(x, t) = -\frac{vl^*}{3}\nabla\rho(x, t), \tag{18}$$

$$l^* = \frac{l}{1 - \langle\cos\theta\rangle}. \tag{19}$$

Eq. (18) shows that the diffusion process tends to smooth the inhomogeneous distribution of energy in the medium, since current flows from regions of high to regions of low energy density. Eq. (19) defines the transport mean free path, which we shall discuss below.

The final step consists of replacing $J(x)$ in eq. (15) by its expression given in (18). This results in

$$\frac{\partial \rho(x, t)}{\partial t} - D\nabla^2\rho(x, t) = \delta(t)\delta(x - x_0), \tag{20}$$

$$D = \frac{vl^*}{3}. \tag{21}$$

D is the diffusion constant of waves in the medium. We note that when single scattering is isotropic, $l^* = l$. When scattering is anisotropic, several scattering events are necessary for the direction of a scattered beam to become independent of that of the initial beam (see Fig. 4), hence l^* can be interpreted as the length scale required for a beam to lose 'memory' of its initial direction when scattering is anisotropic. For a full derivation of all the above equations in the steady-state case, see Kourganoff (1967).

Boundary conditions of the Diffusion Equation

We follow the method of Zhu, Pine & Weitz (1991). First we assume that approximation (14) is also valid at the interface of two media. The basic procedure consists of writing a balance of energy for an element of surface dS of the boundary. We treat three cases that are relevant to our applications and detail the calculations in one case.

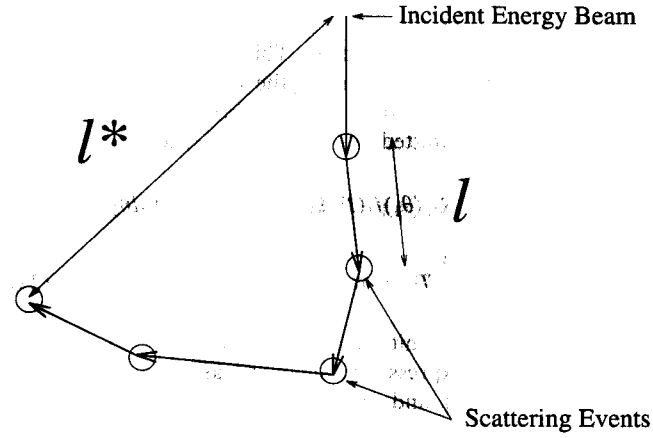

Figure 4. l is the scattering mean free path of waves. It represents the average distance between two scattering events. l^* is the transport mean free path. It is the length scale necessary for a wave packet to loose memory of its initial direction. In the case of isotropic scattering, both are equal.

Case a

Case a is for a perfectly flat interface separating two scattering media with different wave speeds and diffusion constants (see Fig. 5). We use the same notations for the reflection and transmission coefficients and in addition introduce D_i, the diffusion constant of medium i.

The energy amount J^+ flowing per second in the $+z$ direction at a point P of the boundary can be written explicitly in two ways. First, by merely applying the definition of the specific intensity, we obtain the following:

$$J^+ = \int_0^{2\pi} d\phi_1 \int_0^{\pi/2} I_1(P, \Omega_1, t)\cos\theta_1 \sin\theta_1 d\theta_1. \tag{22}$$

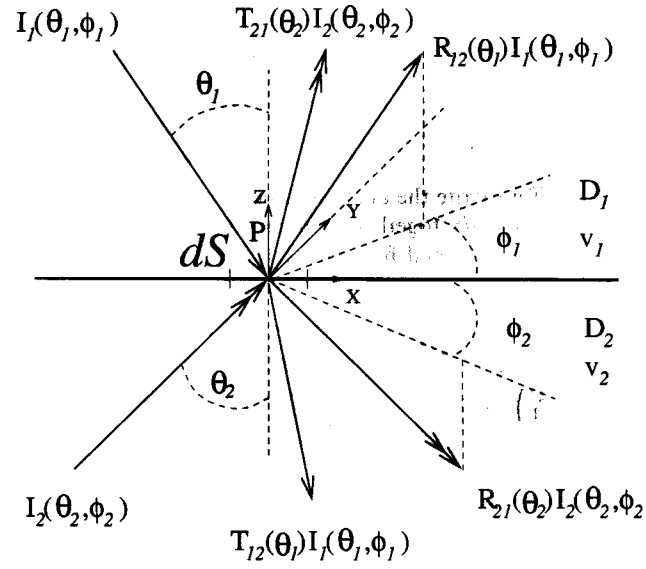

Figure 5. Energy balance at the interface between media 1 and 2. Beam 1 (2) has a single (double) arrow. A beam of intensity $I_i(\theta_i, \phi_i)$ is incident from medium i on a small surface element dS of the boundary of media i and j ($i, j = 1, 2$ and $i \neq j$). θ_i and ϕ_i are the angles of incidence of the beam i in spherical coordinates, the orthonormal reference frame being (x, y, z). The part of beam i reflected in medium i is $R_{ij}I_i$. The part of beam i transmitted in medium j is $T_{ij}I_i$.

The integration is performed over the upper hemisphere of space directions ($\mathbf{\Omega}.z$ is positive). This quantity should equal the flux of medium 1 incident on the interface and reflected back in medium 1, *plus* the flux of medium 2 incident on the boundary and transmitted into medium 1. Hence,

$$J^+ = \int_0^{2\pi} d\phi_1 \int_\pi^{\pi/2} R_{12}(\theta_1) I_1(\boldsymbol{P}, \mathbf{\Omega}_1, t) \cos\theta_1 \sin\theta_1 d\theta_1 + \int_0^{2\pi} d\phi_2 \int_0^{\pi/2} T_{21}(\theta_2) I_2(\boldsymbol{P}, \mathbf{\Omega}_2, t) \cos\theta_2 \sin\theta_2 d\theta_2 , \quad (23)$$

where $\mathbf{\Omega}_1$, $\mathbf{\Omega}_2$ are the unit vectors of directions $(\theta_1, \phi_1), (\theta_2, \phi_2)$ respectively. We express the intensity as specified by the approximation (14) and replace the current vector by its expression (18) and perform the integration over the variable ϕ. Two integrals must be calculated. The first is evident:

$$\int_0^{2\pi} \frac{\rho v}{4\pi} d\phi = \frac{1}{2} \rho v ; \quad (24)$$

the second is

$$\frac{3}{4\pi} \int_0^{2\pi} J(x).\mathbf{\Omega} d\phi = -\frac{v l^*}{2} \frac{\partial \rho}{\partial z} . \quad (25)$$

The integration over θ yields, substituting T_{21} for $(1-R_{21})$,

$$\rho_1 v_1 \left(\frac{1}{2} - C_1\right) - D_1 \frac{\partial \rho_1}{\partial z} (1+3\widetilde{C_1}) = \rho_2 v_2 \left(\frac{1}{2} - C_2\right) - D_2 \frac{\partial \rho_2}{\partial z} (1-3\widetilde{C_2}), \quad (26)$$

where

$$C_j = \int_0^{\pi/2} R_{ji}(\theta) \cos\theta \sin\theta d\theta , \quad (i \neq j)$$

$$\widetilde{C_j} = \int_0^{\pi/2} R_{ji}(\theta) \cos^2\theta \sin\theta d\theta . \quad (28)$$

We must also constrain the component of the current normal to the surface to be conserved, so that

$$D_1 \frac{\partial \rho_1}{\partial z} = D_2 \frac{\partial \rho_2}{\partial z} . \quad (29)$$

Note that if we write the amount of energy flowing in the $-z$ direction across dS together with eq. (26), we can check the conservation of normal flux so that everything is consistent. On introducing

$$\alpha = \frac{\left(\frac{1}{2} - C_2\right)}{\left(\frac{1}{2} - C_1\right)} , \quad (30)$$

$$\beta = 3 \frac{(\widetilde{C_1} + \widetilde{C_2})}{\frac{1}{2} - C_1} , \quad (31)$$

we obtain the following set of boundary conditions:

$$D_1 \frac{\partial \rho_1}{\partial z} = D_2 \frac{\partial \rho_2}{\partial z} \equiv -J , \quad (32)$$

$$\rho_1 v_1 + \beta J = \alpha \rho_2 v_2 . \quad (33)$$

For a random surface, rather than a flat surface, exact boundary conditions of this type can also be written.

Case b

Case b is for a perfectly flat interface separating medium 1, which has a finite diffusion constant, from medium 2, which has an infinite diffusion constant. This is the case when scattering is infinitely weak in medium 2. In such a medium, waves follow straight ray paths, so we only have the Diffusion Equation defined in medium 1. In this case the boundary condition only requires that the incoming flux (the amount of energy flowing across the surface dS in the $+z$ direction) be equal to the internally reflected energy. With

$$\gamma = \frac{2 l_1^*}{3} \frac{(1+3\widetilde{C_1})}{1-2C_1} , \quad (34)$$

one has

$$\rho_1 v_1 + \gamma J = 0 . \quad (35)$$

Case c

The free surface corresponds to an interface across which no energy can flow, thus the boundary condition reads

$$J = 0 . \quad (36)$$

For all the models of Table 1 we are able to describe completely the diffusion of acoustic energy, since we know the governing equation and its boundary conditions. This equation is simpler to solve than the Radiative Transfer Equation because only derivatives are involved. The solutions of the Radiative Transfer Equation should match those of the Diffusion Equation in the limit of large lapse times. The comparison of both helps us to characterize the time- and length scales necessary to be in the diffusive regime, and will be discussed in the next section.

Analytical solution of the Diffusion Equation.

In this section we briefly describe how analytical solutions of the Diffusion Equation have been obtained for models 1–4; final formulae are given in the Appendix. In these four models, one always has the same boundary condition (case c) at the top, and two possible boundary conditions (case a or b) at the base of the layer. The latter depends on the finite or infinite value of the diffusion constant in the half-space. The case of a uniform half-space simply corresponds to $v_1 = v_2$, $D_1 = D_2$, $l_1 = l_2$. The following steps are undertaken. We calculate the Laplace transform with respect to time of the Diffusion Equation and its boundary conditions. We take advantage of the symmetry of the problem by employing cylindrical coordinates. The separation of the variables leads to two Sturm–Liouville differential equations with a delta-like source term in both. The homogeneous differential equations are solved with their boundary conditions matched. Next, the source terms are introduced, which gives the solution of the problem in the complex frequency (Laplace) domain. Finally, the inverse Laplace transform is calculated. It is expressed in terms of a closed contour integral involving a branch cut. The use of the residue theorem enables us to find the solution in closed form. The technique described above is quite general and powerful and is used in various domains of physics to solve

partial differential equations (Morse & Feshbach 1953). We do not reproduce the tedious calculations but they are available to the interested reader.

COMPARISON OF DIFFUSION AND RADIATIVE TRANSFER MODELS

In this section, we analyse the results obtained from analytical solutions of the Diffusion Equation and numerical solutions of the Radiative Transfer Equation. We focus on the characteristics of the diffusion regime and define the domain of validity of the Diffusion Approximation. We assume that the scattering is isotropic in both the half-space and the layer. In all calculations, the source is assumed instantaneous, point-like, isotropic and located just below the free surface. Without loss of generality we assume it to have unit strength. We present tests of convergence of the Radiative Transfer Equation and Diffusion Equation solutions for models 2 and 4. In both models, we have a fixed velocity contrast ($v_1/v_2=0.74$) and hence energy is partially reflected and transmitted at the base of the layer. This is a fundamental change with respect to the uniform half-space (model 1). This ratio of 0.74 corresponds to $v_1=3.5$ km s^{-1} and $v_2=4.7$ km s^{-1}, which are realistic values for the shear-wave velocities in the continental crust and the upper mantle respectively. We recall that in model 2 the mean free path is depth-independent (no mean free path contrast), whilst in model 4 the mean free path takes a very large (infinite limit) value below the layer, that is the ratio l_1/l_2 is equal to zero. This enables us to check our results for two entirely different configurations.

The Diffusion Equation and Radiative Transfer Equation solutions for model 2 have been plotted in Fig. 6. The Radiative Transfer curves can easily be recognized because they exhibit the characteristic ripples caused by incomplete averaging. The source detector distance r varies over the broad range 0–200 km. We consider mean free path values ranging from 10 to 150 km in order to explore different scattering regimes. The diffusion theory predicts the asymptotic behaviour of the Radiative Transfer Equation solutions with a very good precision. Since both calculations are completely independent, this agreement demonstrates the accuracy of our calculations.

For the smallest mean free path value ($l_1=l_2=10$ km), one can see the particular shape of the envelopes computed at large distances, which do not exhibit the familiar monotonic decay

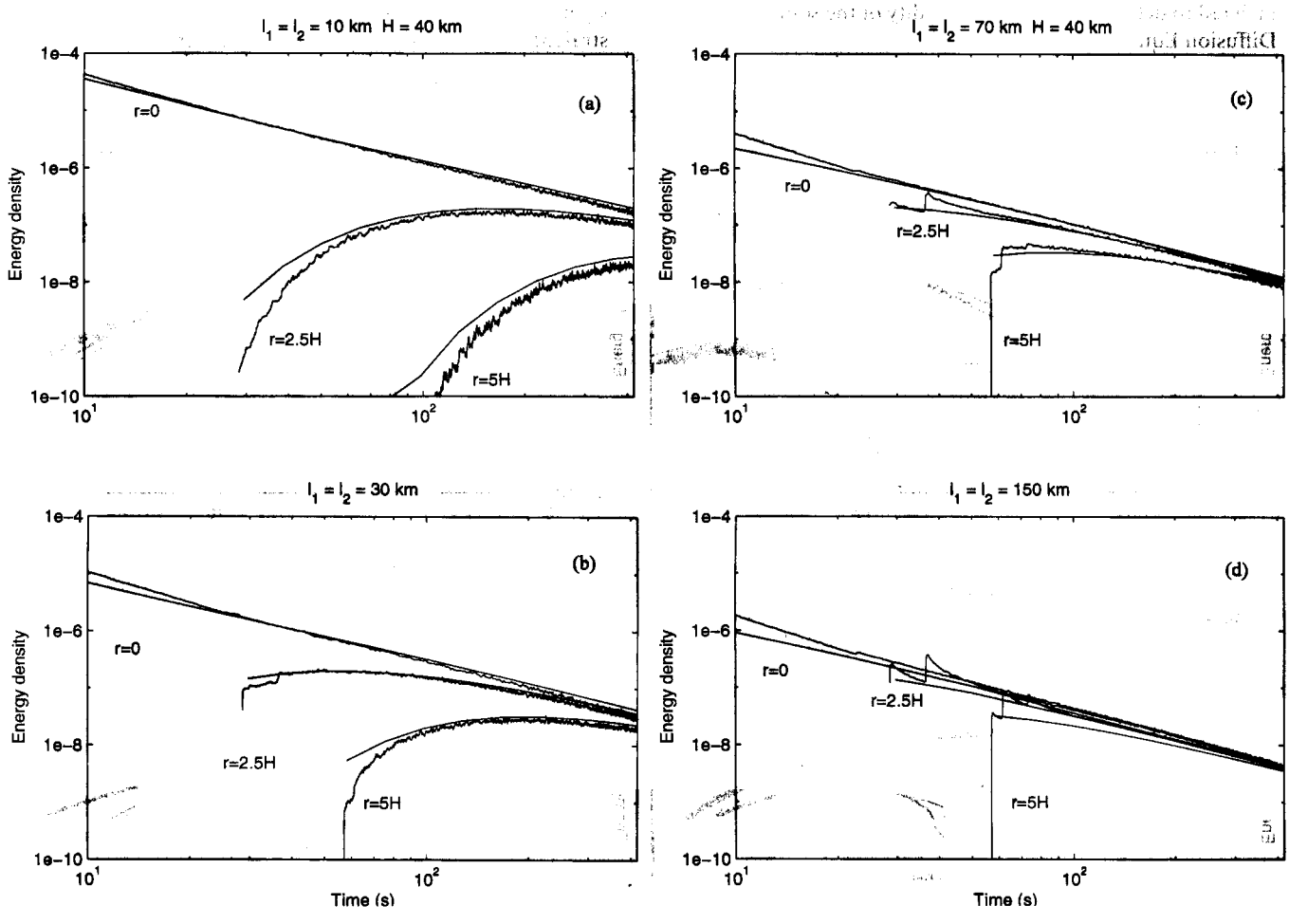

Figure 6. Comparison of the solutions of the Diffusion and Radiative Transfer Equations for model 2, with a layer thickness $H=40$ km. The Radiative Transfer Equation solution curves exhibit characteristic ripples. The mean free path values l_1 (in the upper layer) and l_2 (in the underlying half-space) are indicated at the top of each figure. The source is isotropic, point-like, instantaneous and has unit strength. Source and receivers are located just below the free surface. The time origin corresponds to the energy release at the source. For each curve the source–station distance r is indicated in terms of the upper layer thickness H.

shown in previous studies (e.g. Abubakirov & Gusev 1990; Hoshiba 1995). This difference is explained by the fact that previous theoretical studies of the coda decay concentrated on much smaller epicentral distances ($r \leq 100$ km) and larger mean free paths. In addition, we did not take into account any intrinsic absorption of rocks at all, which would evidently lead to a faster decay. Our method does not have any limitation to the incorporation of an intrinsic attenuation, but in this study we wanted to separate the influence of the mean free path from that of velocity contrast on the coda decay. For a small mean free path ($l = 10$ km) and large epicentral distances ($r > 100$ km), the Radiative Transfer curves show the passage of a diffusion front (Fig. 6a) characteristic of the diffusion regime (e.g. Sheng 1995).

In Fig. 7 we present the envelopes obtained for model 4. When we consider relatively small values of the mean free path (10 km in Fig. 7a, 30 km in Fig. 7b), the solutions of the Diffusion Equation agree very closely with the solutions of the Radiative Transfer Equation. On the other hand, for somewhat larger mean free paths (70 km in Fig. 7c, 150 km in Fig. 7d), we find a significant disagreement between the decay of the Radiative Transfer Equation and that predicted by the Diffusion Equation, especially for large lapse times when the diffusion regime is reached. We need to discuss these results in detail to define the domain of validity of the solutions of the Diffusion Equation.

We introduce the dimensionless parameter H/l_1 in order to keep the discussion as general as possible. We recall that in the derivation of the boundary conditions of the Diffusion Equation we have assumed that the intensity field is almost isotropic, even at the boundaries of the layer. The limitation of this assumption is of particular importance for model 4, where scattering is restricted in a layer of depth H, in particular when $H \approx l_1$. The conditions necessary to reach the diffusion regime at the boundaries will be fulfilled if $H/l_1 \gg 1$ but will be violated if $H/l_1 \ll 1$. Between these two extreme cases, it is not *a priori* obvious that the diffusion model will lead to a correct approximation to the Radiative Transfer Equation solutions. The numerical simulations help us in defining precisely the actual limits of the Diffusion Approximation.

For $H/l_1 = 4$ and $H/l_1 = 1.3$ (Figs 7a and b), the convergence toward the Diffusion Equation is confirmed, independent of the mean free path contrast, and for various source station distances. However, for $H/l_1 = 0.6$ and $H/l_1 = 0.25$ the solutions start to diverge (Figs 7c and d). In the last two cases, the decay predicted by the Diffusion Approximation is clearly faster than that observed for the Radiative Transfer Equation solutions. The explanation for this discrepancy is found in the assumption that the intensity field is isotropic at the boundary between the layer and the half-space. For $H/l_1 = 0.6$ or 0.25, a significant part of the energy emitted by the source follows straight ray paths and directly encounters the inner boundary.

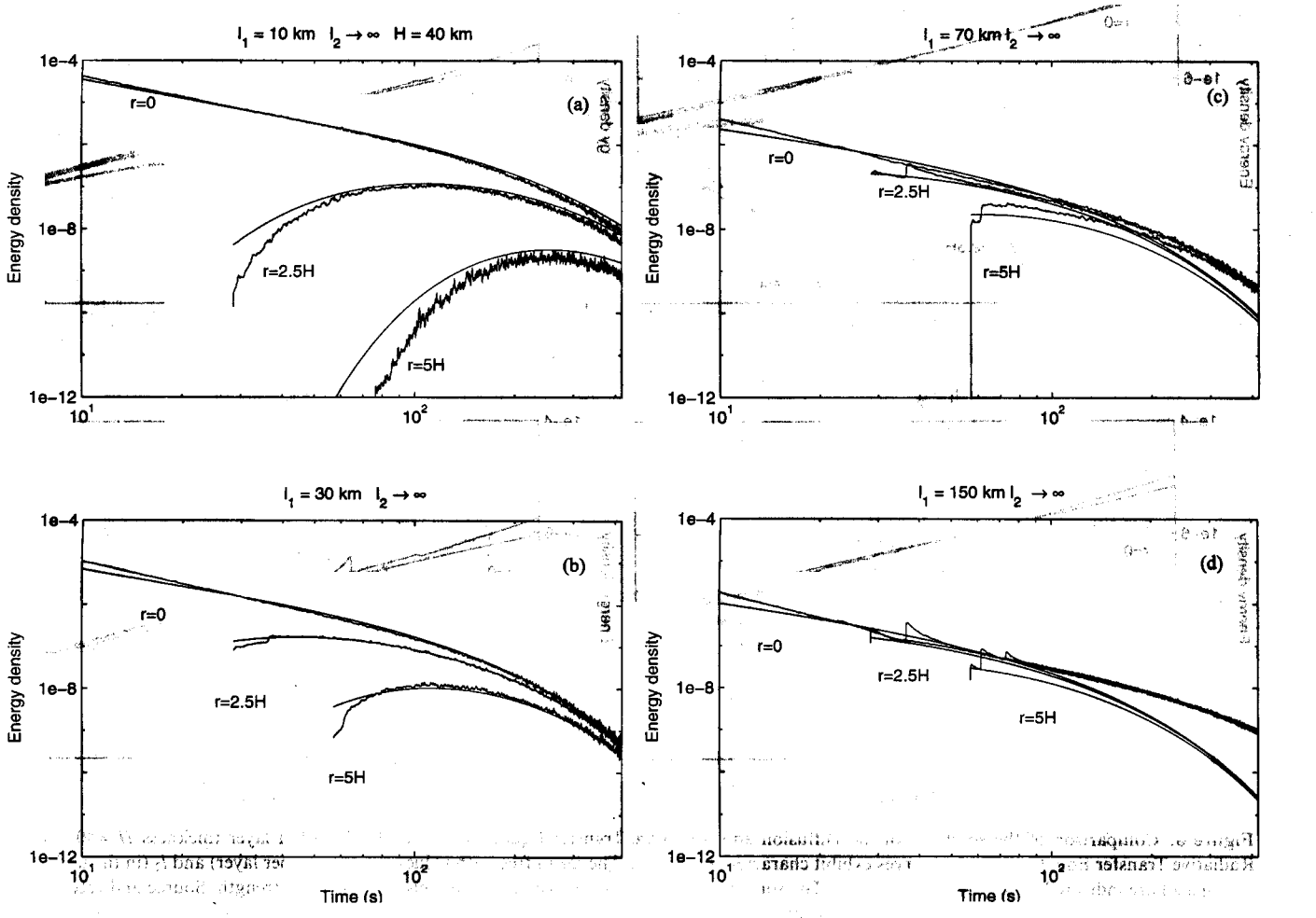

Figure 7. Same as Fig. 6 for model 4.

This is illustrated in Figs 7(c) and (d) by the existence of jumps in the coda amplitude on the Radiative Transfer curves at post-critical distances. Moreover, part of the direct energy incident at the bottom of the layer at pre-critical angles will be irreversibly lost. Therefore, the energy balance at the bottom of the layer is inaccurately described by the Diffusion Approximation, leading to an incorrect asymptotic decay. These arguments do not hold for model 2 because in this model scattering takes place in the whole space. Although some energy is directly transmitted into the half-space, it undergoes other scattering and will be backscattered to the receiver. Hence, the diffusion in the lower half-space, which is well described in our approximation, will finally be the dominant process.

Finally, if $l_1/l_2=1$ (no mean free path contrast), the Diffusion Approximation always turns out to provide a reliable approximation to the Radiative Transfer for large lapse times, while for $l_1/l_2=0$ (strong mean free path contrast), the Diffusion Approximation is valid only when the layer thickness is larger than the mean free path ($H/l_1 > 1$). In the following sections, we focus on some applications of the above results to the observation of coda in continental domains. Scattering has been assumed to be isotropic in all calculations.

EFFECT OF THE VELOCITY STRUCTURE ON THE CODA

In this section we study the effect of a velocity contrast in a medium where the mean free path is independent of depth. To this end, we consider the models 1 and 2. The source is located at the surface and scattering is assumed to be isotropic. Our reference model (model 1) has a uniform speed $v_1=3.5$ km s^{-1}, while in model 2 the velocity jumps to the value $v_2=4.7$ km s^{-1} at depth H. Models 2 and 4 present a simplified model of the continental crust on top of the mantle. The interface between both layers is identified as the Moho. We consider different mean free path values and epicentral distances and show the comparison between models 1 and 2 in Figs 8(a)–(c). In each case, for short lapse times, the envelopes are very close for both velocity models since the different structure can only be

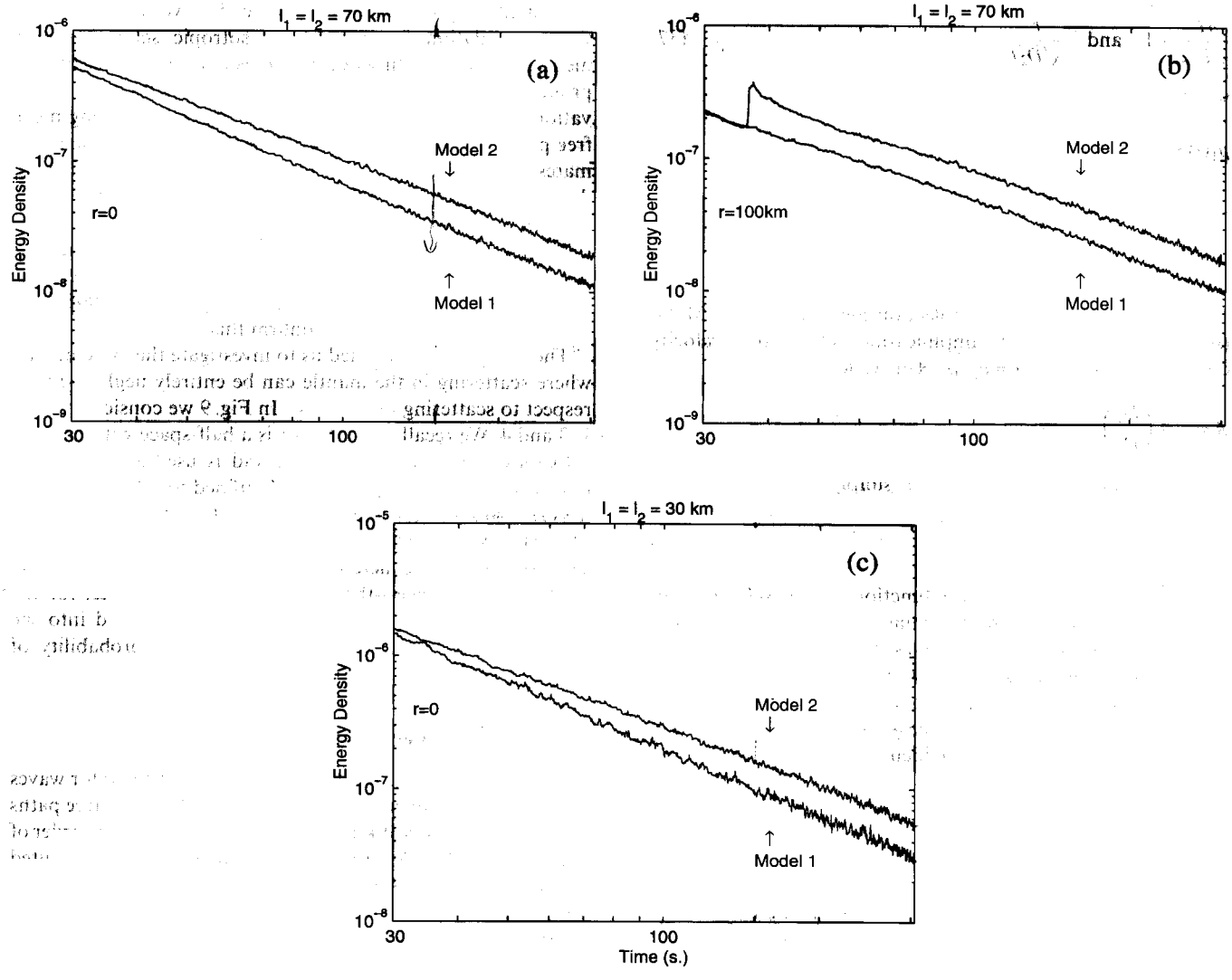

Figure 8. Comparison of the coda for models 1 and 2. The epicentral distance r is given in the figure. In both models, the mean free path is uniform and its value is indicated at the top of each figure. For model 2 the upper layer thickness is $H=40$ km and the velocity contrast is $v_1/v_2=3.5/4.7$. The time origin is the energy release at the source.

appreciated after some energy beams reach depth H and are reflected back to the free surface. For larger lapse times, the curves start to split up: the coda amplitude is larger in model 2. This amplification is due to the trapping of part of the energy in the low-velocity layer, which acts as a waveguide. A comparison of Figs 8(a) and (b) illustrates that the amplification is independent of the distance, while a comparison of Figs 8(a) and (c) shows the amplification to be independent of the mean free path as well. In Fig. 8(b), we note a jump in the coda amplitude for model 2. This jump is created by the total reflection of waves at the Moho beyond the critical angle. Such a discontinuity in the coda decay has already been observed by Obara & Sato (1988), who related it to the existence of a dipping reflector beneath the southern Kanto district in Japan. In each case the curves obtained for the two velocity models finally become parallel and decay as $t^{-3/2}$. This algebraic decay is characteristic of the diffusion regime in a uniform half-space.

The use of the Diffusion Approximation makes it possible to give closed form formulae for the asymptotic decay of the synthetic codas. These analytical solutions of the Diffusion Equation are given in the Appendix. Under the following assumptions:

$$\frac{H}{\sqrt{D_2 t}} \ll 1 \quad \text{and} \quad \frac{r}{\sqrt{D_2 t}} \ll 1, \tag{37}$$

we obtain:

$$\rho_1(t) \sim \frac{1}{4(\pi D_1 t)^{1.5}} \quad \text{for model 1}, \tag{38}$$

whereas

$$\rho_2(t) \sim \frac{\alpha v_2}{4 v_1 (\pi D_2 t)^{1.5}} \quad \text{for model 2}, \tag{39}$$

where α depends only on the reflection coefficients at the Moho (see eqs 27–31). The coda amplification induced by a velocity contrast is defined as $A = \rho_2 / \rho_1$. This yields

$$A = \frac{\alpha v_2}{v_1} \left(\frac{D_1}{D_2} \right)^{3/2}. \tag{40}$$

In the present case, with $l_1 = l_2$, A is simply

$$A = \alpha \sqrt{\frac{v_1}{v_2}}. \tag{41}$$

This amplification factor is a function of the velocity contrast only, as indicated by the numerical Radiative Transfer Equation solutions. In the examples shown in Fig. 8, we found $A \simeq 1.55$ in complete agreement with eq. (41). We have therefore shown that a low-velocity upper layer increases the coda level in a medium where the source is located at the surface and the mean free path is independent of depth. However, in models with jumps in velocity, the asymptotic decay remains of the form $t^{-3/2}$, as is the case for a homogeneous half-space without intrinsic absorption.

The Radiative Transfer Equation solutions for models with equal mean free paths in the crust and mantle might give us a first estimate of the shape of the coda decay in continental areas. However, owing to the different mechanical and chemical properties, crust and mantle are unlikely to have the same mean free path values. The model considered in the next section will give us a more realistic estimate for the possible range of variation in coda decay.

EFFECT OF A STRONG MEAN FREE PATH CONTRAST ON THE CODA

We want to investigate the changes in coda decay induced by a jump of the mean free path at depth H. Several observations indicate that the mantle may be less heterogeneous than the crust. This suggests that the mean free path of the mantle is larger than that of the crust. From a geological viewpoint (see e.g. Fowler 1990), the crust components (sediments, metamorphic rocks, etc.) have very inhomogeneous chemical and mechanical properties, in sharp contrast with the mantle, which is believed to have an almost uniform composition.

From a seismological viewpoint, at least two independent observations tend to confirm our assumption of a weak scattering mantle. First, deep seismic reflection experiments have established a strong reflectivity of the crust, whereas almost no energy is backscattered by the upper mantle. The absence of seismic reflectors in the mantle supports the relative homogeneity of its mechanical properties (Marthelot & Bano 1991). Second, the direct S-wave pulse emitted by local earthquakes exhibits a characteristic broadening as a function of the source–station distance. Abubakirov & Gusev (1990) calculated the pulse duration of direct S waves using a Monte Carlo simulation for multiple anisotropic scattering in a medium with uniform wave velocities and uniform scattering properties. From a comparison of their simulations to observations, they inferred some estimates for the scattering mean free path of waves. They noticed large deviations in their estimates that seem to indicate that a uniform scattering strength does not apply in the Earth's lithosphere. A careful analysis showed that the mean free path seems to increase with the exploration depth of the seismic waves. This lead them to the conclusion that the scattering strength probably strongly decreases with depth. Other studies by Gusev (1995) and Hoshiba (1994) more or less confirm this.

These arguments have led us to investigate the extreme case where scattering in the mantle can be entirely neglected with respect to scattering in the crust. In Fig. 9 we consider models 1, 3 and 4. We recall that model 1 is a half-space with uniform velocities and a mean free path, and is used as a reference model. In model 3, scatterers are confined to a layer of thickness $H = 40$ km, while the velocity is kept constant. In model 4, the velocity mismatch at the Moho is also incorporated. The top layer—the heterogeneous crust—overlying a non-scattering half-space—the mantle—is a crude model for the lithosphere. In these models, any wave transmitted into the mantle propagates downwards and has zero probability of going back to the receiver.

Analysis of synthetic codas

In the following we assume that codas are computed for waves with a central frequency $f = 1$ Hz. We consider mean free paths ranging from 30 to 150 km, that is covering almost one order of magnitude. In Fig. 9, we present the coda envelopes computed for models 1, 3 and 4 detected at 100 km from the source and for a mean free path $l_1 = 30$ km. The early coda is magnified in order to differentiate the curves. For lapse times smaller than the traveltime of the reflection at the Moho (approximately 37 s), the coda amplitudes are the same for the three models because the medium explored by the waves is the same. For model 4, we observe a slight jump in the coda level due to the

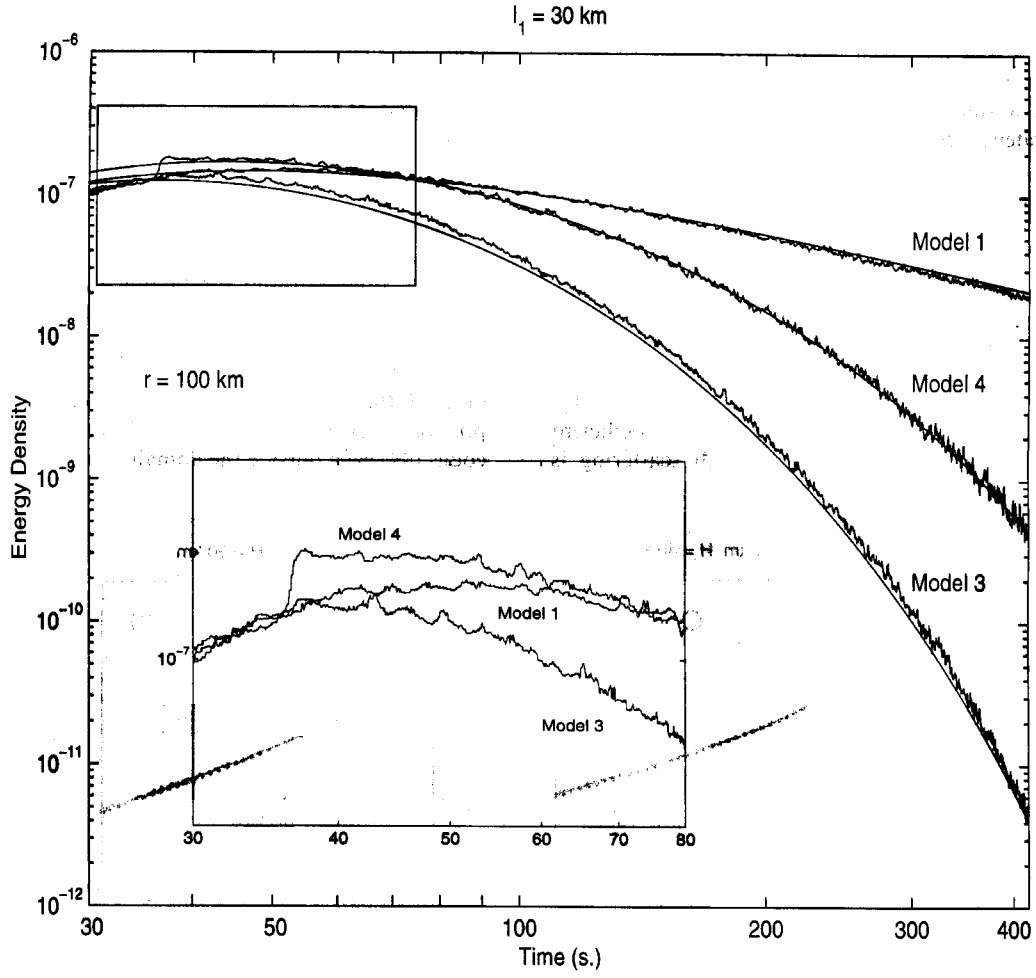

Figure 9. Comparison of models 1, 3 and 4. The Radiative Transfer and Diffusion Equation solutions are plotted. The Radiative Transfer Equation solution curves exhibit characteristic ripples. For models 3 and 4 the scattering is confined to an upper layer of thickness $H = 40$ km. In models 1 and 3 the S-wave velocity is $v_1 = 3.5$ km s^{-1}, whereas in model 4 a velocity contrast $v_1/v_2 = 3.5/4.7$ has been added. The source station distance is $r = 100$ km and the mean free path value is $l_1 = 30$ km for all models. The time origin is the energy release at the source. The start of the signals has been magnified in order to distinguish the evolution of the coda for the three models.

energy reflected at post-critical angles on the Moho. Apart from these details, one must note that the dependences of the energy density on time in models 3 and 4 are very different from those of our reference model 1. Clearly, the decay rate of the envelopes for strong mean free path jumps is much larger than that in the uniform model. This is a direct consequence of the energy losses at the base of the crust in models 3 and 4, as has already been noted by Korn (1990) for energy flux models. In our case, scattering in the mantle is neglected and the mean free path in the crust is of the order of the layer thickness. After a few scatterings, most energy escaped from the crust and disappeared into the mantle. In view of the relatively fast decay rate of model 3 compared to that of model 4, it is important to consider a velocity jump at the Moho in the modelling.

After about 50 s, the Radiative Transfer solutions have converged towards their diffusion asymptotics (Fig. 9). Therefore, we can use the analytical solutions of the Diffusion Equation to give an approximation of the shape of the coda. From the solution of the Diffusion Equation given in the Appendix—retaining the leading term at large times—we obtain the following for model 4:

$$\rho_4(r, t) \sim \exp\left(-\frac{r^2}{4D_1 t}\right) \frac{\exp\left(-D_1 \frac{\xi_0^2}{H^2} t\right)}{HD_1 t}, \tag{42}$$

where ξ_0 denotes the smallest root of the equation

$$\xi \tan \xi = \frac{\gamma}{H}, \tag{43}$$

γ is determined by the reflection coefficient at the Moho (eq. 34), and D_1 is the diffusion constant of waves. When the source and station are close, the first exponential term will rapidly tend to 1 and formula (42) can be rewritten as

$$\rho(t) \sim \frac{1}{t} \exp\left(-\frac{2\pi f t}{Q_c^*}\right), \tag{44}$$

where we have introduced

$$Q_c^* = \frac{2\pi H^2 f}{D_1 \xi_0^2}. \tag{45}$$

Expression (44) has the form proposed by Aki & Chouet (1975, formula 9) and will be discussed below. By Q_0^* we denote the value of Q_c^* at a frequency of 1 Hz.

We can give a simple physical interpretation to eq. (44). The t^{-1} dependence corresponds to the asymptotic decay associated with a diffusion process without absorption in a 2-D medium. Actually, when t is large, the finite thickness of the crust becomes negligible with respect to the large distance travelled by the waves so that the layer can be approximated by a 2-D medium. The exponential factor expresses the energy loss into the mantle due to the waves that reach the Moho below the critical angle. Since each time a scattering event occurs a fraction of the energy initially emitted in the crust is lost in the mantle, the energy density decays exponentially. The decay rate will depend on the reflection coefficient R_{12} since the fraction of energy lost at each scattering is determined by the width of the cone of directions below the critical angle.

Although formula (45) applies only under the restrictive conditions of the Diffusion Approximation discussed earlier, we will now show that the formula (44) is still an excellent approximation for the decay in our computations. Outside the domain of validity of the Diffusion Approximation, Q_0^* is evaluated numerically by a simple regression. In Fig. 10 the solid lines show the numerical solutions of the Radiative Transfer Equation and the broken lines show the curves of regression obtained using formula (44). The mean free path, thickness of the crust and corresponding Q_0^* values are given in Fig. 10. After a delay of about 30 s, the approximate expression (45) fits the numerical solution very closely. Therefore, it is possible to give a simple analytical expression of our synthetic codas (44) even outside the domain of validity of the Diffusion

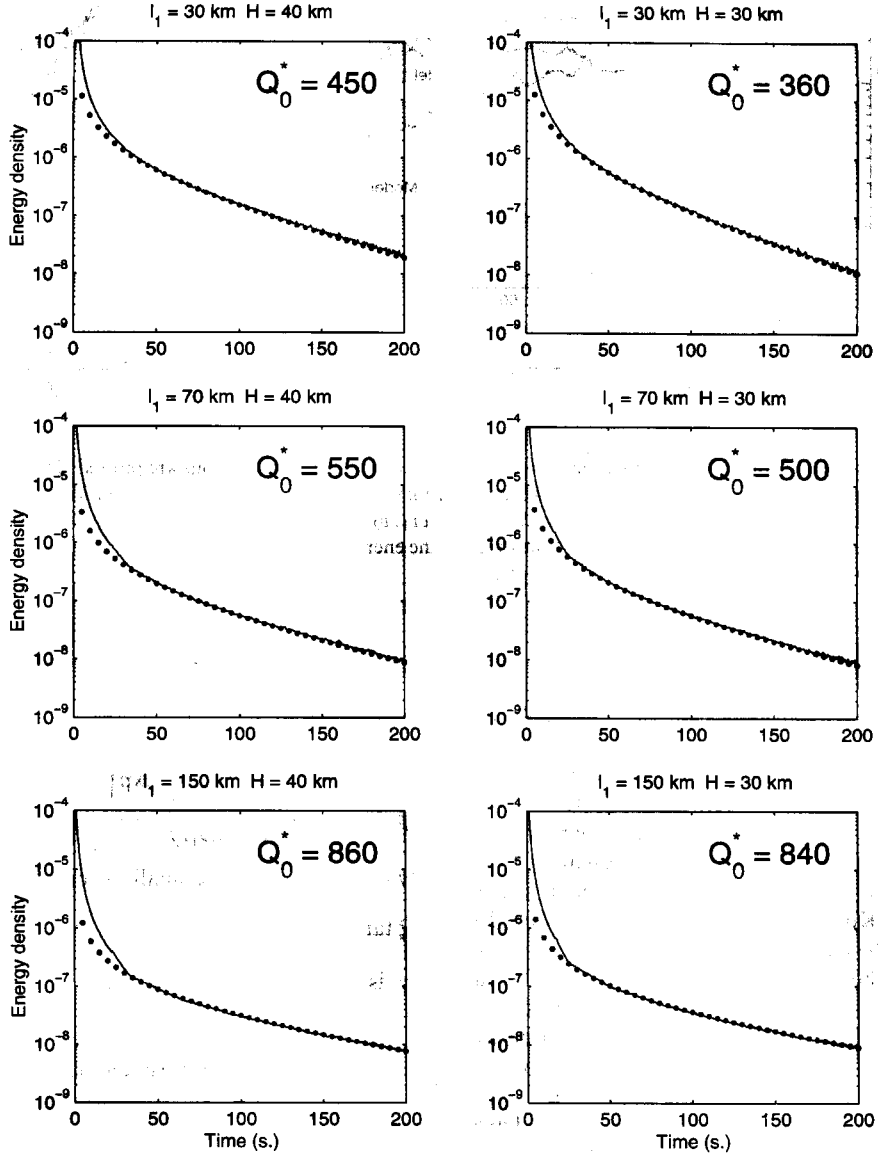

Figure 10. Coda decay obtained for model 4 with $H = 30$ km, $H = 40$ km, and the mean free path of the upper layer l_1 ranging from 30 to 150 km. Solid lines show the numerical solution of the Radiative Transfer Equation, while broken lines show the best approximation obtained with the formula $(1/t)\exp(-2\pi t/Q_0^*)$. The Q_0^* value corresponding to the best approximation is given in the figures. The standard deviation of the Q_0^* is $\Delta Q_0^* \approx 15$.

Approximation. In Fig. 10, with $H=40$ km and $l_1=30$ km, the conditions of application of the Diffusion Approximation are fulfilled and one may check that the Q_0^* evaluated numerically is the same as that obtained from the analytical formula (45).

Comparison of synthetic codas with observations

It is worth noting that formula (42) with $r=0$ has exactly the same form as that proposed by Aki & Chouet (1975, formula 9) to fit the observed codas:

$$\rho(t)\sim\frac{1}{t^n}\exp\left(-\frac{2\pi ft}{Q_c}\right), \tag{46}$$

where $n\in[1, 2]$. While originally derived from simple models, namely single scattering and diffusion in a homogeneous infinite space (Aki & Chouet 1975), this expression has been used extensively to describe the coda decay of actual seismograms because this simple formula fits the observed codas remarkably well (see e.g. Herraiz & Espinosa 1987 for a review). Therefore, Q_c (coda Q) emerged as a very useful parameter that measures the decay rate of observed codas in a defined area. Globally, the Q_c measurements can be summarized as

$$Q_c=Q_0 f^v, \tag{47}$$

where $50<Q_0<1000$ and $0<v<1$. Hereafter, we will not discuss the frequency dependence of Q_c, but rather focus on its value around 1 Hz. The lower bound for Q_0 is probably of the order of $Q_0=50$, as found in Mexico by Rodriguez, Havskov & Singh (1983). The upper bound is probably larger than 1000 as measured in central China by Jin & Aki (1988). Several extensive studies of Q_0 can be found in the literature (e.g. Singh & Herrmann 1983; Jin & Aki 1988; Oancea, Bazacliu & Mihalache 1991) that show large variations of Q_0 depending on the geological environment.

The physical interpretation of Q_c and its relation to scattering and intrinsic absorption of the lithosphere are still actively debated. Among recent papers are those by Abubakirov & Gusev (1990), Hoshiba (1993, 1994) and Gusev (1995). In the previous section, we have shown that a formula similar to (46) is expected in a layered elastic model with a strong mean free path contrast. Since the observed and synthetic coda decay have the same expression, we can directly compare Q_0 and Q_0^* in order to evaluate the importance of the leakage effect we have described. We note that, depending on the authors, the value of the exponent n used in Q_c measurements ranges from 1 to 2. However, as already pointed out in Rautian & Khalturin (1978) and Jin & Aki (1988), the choice of n has a minor effect on the Q_c value, since in eq. (46) the exponential factor dominates over the algebraic factor. Let us compare the observations with our results for a mean free path larger than the thickness of the crust, which is a reasonable assumption for short-period waves in the Earth's crust. We found that Q_0^* increases for increasing values of the mean free path. With a layer thickness $H=40$ km, Q_0^* ranges from 450 to 860, while for $H=30$ km, Q_0^* ranges from 360 to 840. The quality factor Q_0^* which describes the leakage of energy in a purely elastic model is of the same order as those measured. This demonstrates that the leakage effect has to be considered as a real physical origin for the observed decays, yet the existence of a velocity jump at some depth has to be incorporated, as is evident from Fig. 9.

When the mean free path is much larger in the mantle than in the crust, the leakage of energy into the mantle has some important implications for the interpretation of Q_c. Hoshiba (1993), for instance, applying the results of the Radiative Transfer theory to a lithosphere model with uniform mean free path, absorption and wave speed, inferred the seismic albedo values for Japan. The albedo measures the relative importance of the two processes responsible for the wave attenuation: anelasticity on the one hand and scattering on the other. From his models Hoshiba deduced that in the 1–2 Hz frequency band, the albedo values should be as small as 0.3–0.7. Albedo values <0.5 indicate that anelasticity dominates over scattering. However, Gusev (1995) pointed out that, in uniform and purely elastic lithosphere models, the discrepancy between observations and models can only be ascribed to anelastic absorption. The consideration of the loss of scattered energy into the mantle offers a rather attractive alternative for resolving this discrepancy. To our knowledge, such partial leakage has always been neglected in previous analyses of the coda decay, leading to an overestimation of anelastic absorption.

CONCLUSIONS

We have used both Monte Carlo simulations of the Radiative Transfer Equation and analytical solutions of the Diffusion Equation to model multiple scattering of seismic waves in media including a surficial layer. In models with a uniform mean free path, the solution of the Diffusion Equation proves to be a good approximation to the Radiative Transfer model and gives the exact asymptotic solution. If scattering is confined to a layer, the validity of the solution of the Diffusion Equation proposed is limited to the case where the thickness of the layer is larger than the mean free path of waves.

In media with a constant mean free path, a low-velocity top layer amplifies the coda signal with respect to a half-space with uniform wave speed. The amplification factor is a function of the velocity contrast and the reflection coefficient of waves only. Nevertheless, the energy density still decays asymptotically as $t^{-3/2}$, as is the case for diffuse waves in a homogeneous half-space. We have considered media where scattering is confined to a layer, which is not unrealistic for the Earth. The synthetic coda decays as $(1/t)\exp(-2\pi ft/Q_c^*)$. In the regime of the Diffusion Approximation one obtains the simple relation $Q_c^*\approx(H^2 2\pi f)/(Dt_0^2)$, which establishes a link between the parameter Q_c^* in our model and the diffusion constant of waves. Q_c^* is also a function of the reflection coefficient at the base of the layer, the frequency of waves and the layer thickness. In our model, the Earth's crust is responsible for trapping the scattered energy near the surface, which enables the formation of a coda, even in the absence of scattering in the mantle. Neglecting the possibility of an energy leakage into the mantle in the interpretation of the coda decay may lead to a serious underestimation of the seismic albedo. The model proposed here, based on the assumption of a heterogeneous and scattering crust overlying a rather homogeneous mantle, offers a new alternative physical interpretation of coda Q.

ACKNOWLEDGMENTS

We are indebted to F. Roch and C. Pequegnat for the parallelization of the C code. Fruitful discussions with

N. Shapiro, J. Turner and R. Maynard are greatly appreciated. We thank K. Aki, M. Hoshiba, M. Korn and G. Müller for their helpful and critical comments on an earlier version of the manuscript. The numerical simulations have been performed on the SP-1 computer at the Institut de Mathématiques Appliquées de Grenoble and the Centre de Calcul Intensif de l'Observatoire de Grenoble. This work was supported by the GDR 'POAN' in France.

REFERENCES

Abubakirov, I.R. & Gusev, A.A., 1990. Estimation of scattering properties of lithosphere of Kamchatka based on Monte-Carlo simulation of record envelope of a near earthquake, *Phys. Earth planet. Inter.*, **64**, 52–67.

Aki, K. & Chouet, B., 1975. Origin of coda waves: source, attenuation and scattering effects, *J. geophys. Res.*, **80**, 3322–3342.

Burridge, R. & Papanicolaou G.C., 1975. Transport equations for Stokes' parameters from Maxwell's equations in a random medium, *J. math. Phys.*, **16**, 2074–2085.

Chandrasekhar, S., 1950. *Radiative Transfer*, Van Nostrand, NJ.

Fowler, C.M.R., 1990. *The Solid Earth*, Cambridge University Press, Cambridge.

Frisch, U., 1968. Wave propagation in random media, in *Probabilistic Methods in Applied Mathematics*, Vol. 1, pp. 75–198, ed. Bharucha-Reid, A.T., Academic, New York, NY.

Gusev, A., 1995. Vertical profile of turbidity and coda Q, *Geophys. J. Int.*, **123**, 665–672.

Herraiz, M. & Espinosa, A.F., 1987. Coda waves: a review, *Pure appl. Geophys.*, **125**, 499–577.

Hoshiba, M., 1991. Simulation of multiple scattered coda wave excitation based on the energy conservation law, *Phys. Earth planet. Inter.*, **67**, 123–136.

Hoshiba, M., 1993. Separation of scattering attenuation and intrinsic absorption in Japan using the multiple lapse time window analysis of full seismogram envelope, *J. geophys. Res.*, **98**, 15 809–15 824.

Hoshiba, M., 1994. Simulation of coda wave envelope in depth dependent scattering and absorption structure, *Geophys. Res. Lett.*, **21**, 2853–2856.

Hoshiba, M., 1995. Estimation of nonisotropic scattering in western Japan using coda waves envelopes: application of a multiple non-isotropic scattering model, *J. geophys. Res.*, **100**, 645–657.

Hoshiba, M., 1997. Seismic coda wave envelope in depth dependent S-wave velocity structure, *Phys. Earth planet. Inter.*, **104**, 15–22.

Jin, A. & Aki, K., 1988. Spatial and temporal correlation between coda Q and seismicity in China, *Bull. seism. Soc. Am.*, **78**, 741–769.

Korn, M., 1990. A modified energy flux model for lithospheric scattering of teleseismic body waves, *Geophys. J. Int.*, **102**, 165–175.

Kourganoff, V., 1967. *Introduction à la Théorie Générale du Transfert des Particules*, Gordon & Breach.

Lux, I. & Koblinger, L., 1991. *Monte Carlo Particle Transport Methods: Neutron and Photon Calculations*, CRC Press, Paris.

Marthelot, J.M. & Bano, M., 1991. Lateral variations in crustal reflectivity beneath the Paris Basin, *Tectonophysics*, **173**, 425–434.

Morse, P.M. & Feshbach, H., 1953. *Methods of Theoretical Physics*, Vols 1 & 2, McGraw Hill, New York, NY.

Oancea, V., Bazacliu, O. & Mihalache, G., 1991. Estimation of the coda quality factor for the Romanian territory, *Phys. Earth planet. Inter.*, **67**, 87–94.

Obara, K. & Sato, H., 1988. Existence of an S wave reflector near the upper plane of the double seismic zone beneath the southern Kanto district, Japan, *J. geophys. Res.*, **93**, 15 037–15 045.

Rautian, T.G. & Khalthurin, V.I., 1978. The use of coda for determination of the earthquake source spectrum, *Bull. seism. Soc. Am.*, **68**, 923–948.

Rodriguez, M., Havskov, J. & Singh, S.K., 1983. Q from coda waves near Petatlan, Guerrero, Mexico, *Bull. seism. Soc. Am.*, **73**, 321–326.

Rytov, S.M., Kravtsov, Yu.A. & Tatarskii, V.I., 1989. 4. Wave propagation through random media, in *Principles of Statistical Radiophysics*, Springer-Verlag, Berlin.

Ryzhik, L.V., Papanicolaou, G.C. & Keller, J.B., 1996. Transport equation for elastic and other waves in random medium, *Wave Motion*, **24**, 327–362.

Sato, H., 1995. Formulation of the multiple non-isotropic scattering process in 3-D space on the basis of the energy transport theory, *Geophys. J. Int.*, **121**, 523–531.

Sheng, P., 1995. *Introduction to Wave Scattering, Localization, and Mesoscopic Phenomena*, Academic Press, New York, NY.

Singh, S. & Herrmann, R.B., 1983. Regionalization of crustal coda Q in the continental United States, *J. geophys. Res.*, **88**, 527–538.

Turner, J.A. & Weaver, R.L., 1994. Radiative Transfer and multiple scattering of diffuse ultrasound in polycrystalline media, *J. acoust. Soc. Am.*, **96**, 3675–3683.

Zeng, Y., Su, F. & Aki, K., 1991. Scattering wave energy propagation in a random isotropic scattering medium—I theory, *J. geophys. Res.*, **96**, 607–619.

Zhu, J.X., Pine, D.J. & Weitz, D.A., 1991. Internal reflection of diffusive light in random media, *Physical. Rev. A*, **44**, 3948–3959.

APPENDIX A: SOLUTIONS OF THE DIFFUSION EQUATION

We briefly recall the diffusion equation and the boundary conditions associated with our models. We note that the energy flux always vanishes at the free surface ($z=0$):

$$\frac{\partial \rho(\boldsymbol{x},t)}{\partial t} - D\nabla^2 \rho(\boldsymbol{x}, t) = \delta(t)\delta(\boldsymbol{x}-\boldsymbol{x}_0), \tag{A1}$$

$$J=0 \quad \text{at} \quad z=0, \tag{A2}$$

where J denotes the energy flux. In the following we assume that the focal depth is $z_0=0$ and denote the epicentral distance by r.

Model 1 (half-space)

The solution is easily deduced from the infinite-space solution by the method of images:

$$\rho(r, t) = \frac{1}{4(\pi D_1 t)^{3/2}} \exp\left(-\frac{r^2}{4D_1 t}\right). \tag{A3}$$

Model 2 with $D_2 > D_1$ $\mathcal{A} \simeq H$

The boundary conditions required at the interface of two media differing in their diffusion constant is

$$\text{at } z=H \begin{cases} D_1 \dfrac{\partial \rho_1}{\partial z} = D_2 \dfrac{\partial \rho_2}{\partial z} = -J, \\ \rho_1 v_1 + \beta J = \alpha \rho_2 v_2; \end{cases} \tag{A4}$$

α and β are defined in eqs (30) and (31) respectively. The solution is composed of a double integral and a simple integral over an infinite sum of residues. Note that the number of residues depends on the x variable and becomes infinite as x goes to infinity:

$$\rho(r, t) = \frac{1}{\pi} \int_0^\infty dx x^2 J_0(xr) \left(A(x) + \frac{v_2}{2\pi v_1} B(x) \right), \tag{A5}$$

where J_0 denotes the Bessel function of order 0.

$$A(x) = \sum_{n(x)} \frac{\left[\left(\frac{s_n}{\delta} - 1 \right) Q_n^2 + l^2 (1 - s_n) \right] \sqrt{1 - s_n} \exp(-D_2 x^2 s_n t)}{l(1-\delta) Q_n + \left(xd \left[\left(\frac{s_n}{\delta} - 1 \right) Q_n^2 + l^2 (1 - s_n) \right] - \frac{1}{3} \beta l_2^* \delta l \left(\frac{s_n}{\delta} - 1 \right) \right) \sqrt{1 - s_n}}, \tag{A6}$$

$$B(x) = \int_1^\infty ds \frac{\alpha \sqrt{s-1} \exp(-D_2 x^2 s t)}{C(x, s)}, \tag{A7}$$

$$C(x, s) = \frac{\alpha^2}{l^2} \left(\frac{s}{\delta} - 1 \right) \sin^2 \left(xd \sqrt{\frac{s}{\delta} - 1} \right) + (s-1) \left[\cos \left(xd \sqrt{\frac{s}{\delta} - 1} \right) - \frac{x \beta l_2^*}{3l} \sqrt{\frac{s}{\delta} - 1} \sin \left(xd \sqrt{\frac{s}{\delta} - 1} \right) \right]^2, \tag{A8}$$

where the following notations have been introduced:

$$\delta = \frac{D_1}{D_2}, \quad l = \frac{l_2^*}{l_1^*}, \tag{A9}$$

$$Q(s) = \alpha + \frac{l_2^* x \beta}{3} \sqrt{1 - s}, \tag{A10}$$

$$Q_n = Q(s_n). \tag{A11}$$

The s_n are the roots of the following equation:

$$\tan \left[xd \sqrt{\frac{s}{\delta} - 1} \right] = \frac{l}{Q(s)} \sqrt{\frac{1 - s}{\frac{s}{\delta} - 1}}, \quad \delta < s < 1. \tag{A12}$$

The summation for a given x is indicated by $\sum_{n(x)}$. The number of residues that contribute to the simple integral increases with x. For

$$xd \sqrt{\frac{1}{\delta} - 1} < \frac{\pi}{2},$$

one has only one solution, s_1, but for

$$xd \sqrt{\frac{1}{\delta} - 1} \gg 1,$$

many solutions $s_1, s_2, \ldots, s_n, \ldots$ exist.

Models 3 and 4

These models correspond to the limiting case $D_2 \to \infty$. The boundary conditions at the interface of a diffusing and a non-diffusing medium are

$$\rho_1 v_1 + \gamma J = 0 \quad \text{at} \quad z = H; \tag{A13}$$

γ is defined in eq. (34). The final formula simplifies to a sum of residues:

$$\rho(r,t)=\frac{\exp\left(-\frac{r^2}{4D_1t}\right)}{2\pi HD_1t}\sum_n \frac{\sin\xi_n+\frac{t_n\gamma}{H}\cos\xi_n}{\left(1+\frac{\gamma}{H}\right)\sin\xi_n+\frac{t_n\gamma}{H}\cos\xi_n}\exp\left(-D_1\frac{\xi_n^2}{H^2}t\right), \tag{A14}$$

where the ξ_n are the roots of the equation

$$\xi_n\tan\xi_n=\frac{H}{\gamma}, \quad \xi_n\in\left]n\pi, n\pi+\frac{\pi}{2}\right[, \quad n\in\mathbb{N}. \tag{A15}$$